Concentration Fluctuation Enhancement in Polymer Solutions by Extensional Flow

Jan W. van Egmond† and Gerald G. Fuller*

Department of Chemical Engineering, Stanford University, Stanford, California 94305-5025

*Received February 23, 1993; Revised Manuscript Received October 4, 1993**

ABSTRACT: When subjected to flow, various polymer solutions undergo an "apparent" change of phase, which is manifested by a dramatic increase in the turbidity. This phenomenon is the result of anisotropic flow-induced growth of concentration fluctuations, which can be predicted qualitatively by the coupled equations of motion for the concentration and velocity fields. We have investigated the growth of concentration fluctuations of poor and near-Θ semidilute solutions of polystyrene in dioctyl phthalate (PS/DOP) subject to plane extensional flow at temperatures above the quiescent cloud point. Scattering dichroism and small-angle light scattering (SALS) indicate that concentration fluctuations grow perpendicular to the principal axis of extension for low strain rates. For higher extensional rates, fourfold symmetry appears in the structure factor, with intensity maxima on the axes at 45° to the principal axes. This fourfold symmetry is predicted by a recent theoretical model. We also show that the strength of flow-induced scattering is linear to first order in the ratio of viscoelastic stress to osmotic pressure.

1.0. Introduction

When semidilute polymer solutions at temperatures just above a phase boundary are subjected to flow, they can become turbid. This phenomenon has been reviewed by various authors[1-3] and is sometimes interpreted as a manifestation of a shift in the coexistence curve. For example, Ver Strate and Philippoff[4] have observed that PS/DOP becomes turbid in capillary tube and Couette cell flows at temperatures up to 35 °C above the quiescent coexistence curve at shear rates of approximately 100 s^{-1}. Rangel-Nafaile *et al.*[1] have observed an increase in the cloud point temperature of up to 25 °C in a PS/DOP solution in Poiseuille and steady shear flow in a cone and plate geometry.

Recently, several groups have demonstrated flow-induced turbidity to be the result of an anisotropic enhancement of concentration fluctuations due a coupling of the local viscoelastic stress of entangled polymers with spatial inhomogeneity in monomer concentration.[5-10] Almost without exception, recent work has focused on one particular system: a semidilute solution of PS/DOP. Various time-dependent and steady-state scattering experiments have been performed on PS/DOP solutions in simple shear flow.[5-8] The general observation has been that for low shear rates (Wi < 1, where Wi is the Weissenberg number), butterfly scattering patterns develop. Two lobes of high scattering intensity on an axis parallel to the principal axis of the polymeric stress develop. The direction of greatest concentration gradient is thus parallel to the principal stress axis. For simple shear, concentration fluctuation dynamics have been investigated in the flow/vorticity and flow/velocity-gradient planes. In the parallel plate and cone and plate geometries, maximum scattering is in the flow direction and hence elongated domains of high concentration grow along the vorticity direction.[6] In the flow/velocity-gradient plane high-intensity lobes are oriented with the long axis between 135 and 90° to the flow direction.[5,6] Furthermore, the directions of birefringence and dichroism are perpendicular to each other, indicating that concentration fluctuations are elongated perpendicular to the major axis of the stress.[9] At high shear rates, various nonlinear phenomena have been observed. In the parallel plate geometry above a critical shear rate, dichroism revealed that concentration fluctuations rotated through 90° and oriented in the flow direction.[10] Near this critical shear rate, rheological measurements also revealed large shear-thickening behavior. At still higher shear rates, large time-dependent fluctuations in birefringence and dichroism appear. It is feasible that shear-thickening and the time-dependent fluctuations are induced by a nonlinear coupling between concentration fluctuations and the local flow field.

This paper extends the investigation of flow-enhanced scattering patterns to plane extensional flow. In this flow, four-lobed small-angle light scattering patterns develop. We show that these patterns qualitatively match the predictions of a recent model. Other types of flow-induced structural changes in extensional flows have been reported in the literature. In extensional and shear flows, flow-induced crystallization has been observed for polymer solutions and melts.[11-13] Stress-induced crystallization has also been studied using birefringence and light scattering.[14] Flow-induced miscibility enhancement has been observed for a polymer blend of polystyrene with poly(vinyl methyl ether) in extensional flow.[15] In their review of extensional flow-induced phenomena in polymer systems, Keller and Odell[16] report extensional flow-induced gelation in poly(styrenesulfonate) in solution with $CaCl_2$. Birefringence studies in extensional flows have also been conducted by Leal and co-workers.[17,18]

2.0. Theory

The behavior of shear-enhanced scattering patterns is in qualitative agreement with a hydrodynamic model developed by Helfand and Fredrickson[19] (HF). Onuki,[20-22] Doi,[23,24] and Milner[25] have developed similar models based on the two-fluid model of de Gennes.[26] These models include a coupling of fluctuations in monomer concentration $\phi(\mathbf{r},t)$, velocity $\mathbf{u}(\mathbf{r},t)$, and stress $\tau(\mathbf{r},t)$ through a Langevin equation for mass transport, the Navier–Stokes equations, and a constitutive equation relating polymeric stress to rate of strain. The system of equations describing the rate of change of the velocity and concentration fields

† Present address: Department of Chemical Engineering, University of Massachusetts, Amherst, MA 01003.

* Abstract published in *Advance ACS Abstracts*, November 15, 1993.

0024-9297/93/2226-7182$04.00/0

is similar to models for critical dynamics in binary fluids,[27] except that a term for elasticity is added. Central to the HF and other models is the dependence of transport coefficients on local concentration. This results in coupled equations of change for concentration and local stress and induces anisotropic growth of concentration fluctuations in an anisotropic flow field. A critical assumption in HF[19] is that the time scale of stress relaxation τ_r is much smaller than the concentration fluctuation relaxation time ξ^2/D, where D is the cooperative diffusion coefficient and ξ is the correlation length associated with concentration fluctuations.

Counteracting flow enhancement of concentration fluctuations is the osmotic pressure π. If the free energy per unit volume f is described by the Flory–Huggins expression, then for $1/N \ll \phi \ll 1$, where N is the number of monomers per chain, we have[28]

$$\frac{\partial \pi}{\partial \phi} = \phi \frac{\partial^2 f}{\partial \phi^2} \approx (k_B T/a^3)(1 - 2\chi)\phi \tag{1}$$

Here a is the monomer size, k_B is Boltzmann's constant, and χ is the interaction parameter. Local concentration is expressed in terms of the average concentration $\langle \phi \rangle = \phi^\circ$ and the local fluctuation $\phi'(\mathbf{r},t)$. The polymeric stress is given by the second-order fluid model, as was originally assumed in the HF model.[19] While a constitutive equation such as the Oldroyd-B[3] model would be more appropriate than the second-order fluid, the latter model seems to predict steady-state behavior in a relatively simple and qualitatively accurate manner. Polymer viscosity η_p and the first and second normal stress coefficients (Ψ_1 and Ψ_2) are assumed to be concentration dependent up to first order in concentration fluctuation ($\eta_p(\phi) = \eta_p^\circ + \eta_p'\phi'$ and $\Psi_i(\phi) = \Psi_i^\circ + \Psi_i'\phi'$). Fluctuations in transport coefficients result in a fluctuating stress ($\tau(\mathbf{r}) = \tau^\circ + \tau'(\mathbf{r})$). Assuming that relaxation times for concentration fluctuations are larger than those for velocity fluctuations $\mathbf{u}'(\mathbf{r})$ and polymeric stress fluctuations $\tau'(\mathbf{r})$, the model may be solved in terms of the structure factor.

For a two-dimensional extensional flow field $\mathbf{u}^\circ = \dot{\epsilon}(x,-y,0)$, where $\dot{\epsilon}$ is the extensional rate, the HF model can be solved in Fourier space ($\mathbf{k}$-space) to obtain the time-dependent structure factor[30] $S(\mathbf{k},t) \equiv \langle \hat{\phi}'(\mathbf{k},t)\, \hat{\phi}'^*(\mathbf{k},t) \rangle$ given by

$$\frac{\partial S}{\partial t} = \dot{\epsilon}\left(k_x \frac{\partial}{\partial k_x} - k_y \frac{\partial}{\partial k_y}\right)S - 2\left(\frac{Da^3}{k_B T}\right)k^2\left[\frac{\partial^2 f}{\partial \phi^2} + Kk^2 - \mathbf{ll}:\frac{\partial}{\partial \hat{\phi}}\hat{\tau}'\right]S + 2Dk^2 \tag{2}$$

The cooperative diffusion coefficient is $D/k_B T = \zeta^{-1}$, where ζ is the monomer mobility. K depends on the correlation length of concentration fluctuations $\xi = [K/(k_B T/a^3)]^{1/2}$. Equation 2 governs the dynamics of concentration fluctuations and predicts the enhancement of concentration fluctuations, turbidity, anisotropic scattering patterns, and scattering dichroism. In the limit where diffusion dominates convection, $Dk^2 > \dot{\epsilon}$, the steady-state structure factor is simply

$$S(\mathbf{k})^{-1} \sim \frac{\partial^2 f}{\partial \phi^2} + Kk^2 - \mathbf{ll}:\frac{\partial}{\partial \hat{\phi}}\hat{\tau}' \tag{3}$$

which has the form of a quiescent Ornstein–Zernike[31] structure factor modified by the anisotropic fluctuating stress projection $\mathbf{ll}:\frac{\partial}{\partial \hat{\phi}}\hat{\tau}'$, where $\mathbf{l} \equiv \mathbf{k}/|\mathbf{k}|$ and

$$\mathbf{ll}:\hat{\tau}' = \left[2\eta_p'(l_x^2 - l_y^2)\dot{\epsilon} + (2\Psi_1' + 4\Psi_2')\dot{\epsilon}^2 - \frac{4\eta_p'(2\Psi_1^\circ + 8\Psi_2^\circ)\dot{\epsilon}^2 l_x^2 l_y^2}{\eta_s + \eta_p^\circ}\right]\hat{\phi}'(\mathbf{k}) \tag{4}$$

Here η_s is the solvent viscosity. The first term corresponds to enhancement of fluctuations perpendicular to the direction of extension at an angle $\varphi = 90°$ to the x-axis. The result is enhanced scattering parallel to the principal axis of the stress tensor. On the other hand, suppression of fluctuations is predicted along the extensional axis (x-axis) due to a coupling between concentration and viscosity. The second term of eq 4 predicts an increase in scattering for all $\mathbf{k}$ if $2\Psi_1' + 4\Psi_2'$ is positive, as would usually be the case in solutions and blends. The third term predicts a four-lobed scattering pattern through the factor $l_x^2 l_y^2$. This term is the result of secondary flow effects and has been truncated to second order in $\dot{\epsilon}$. Secondary flow contributions should dominate at high extensional rates and arise from fluctuating stresses required for continuity to be satisfied. Indeed a fluctuating shear stress arises:

$$\hat{\tau}_{xy}' = (\eta_p^\circ - \Psi_1^\circ)ik_y\hat{u}_x' + (\eta_p^\circ + \Psi_1^\circ)ik_x\hat{u}_y' \tag{5}$$

While the base shear stress τ_{xy}° vanishes due to symmetry, the fluctuating shear component does not obey symmetry requirements.

Ignoring solvent stress contributions, eq 3 is made dimensionless with respect to the polymeric stress $\eta_p^\circ\dot{\epsilon}$. The structure factor then depends on five dimensionless parameters:

$$S(\tilde{\mathbf{k}}) \sim \frac{1}{1 + \tilde{k}^2 - O_s\tilde{T}} \tag{6}$$

where O_s is the ratio of the stress $\eta_p^\circ\dot{\epsilon}$ to the osmotic pressure. The scattering vector $\tilde{k} = [K/(\partial^2 f/\partial\phi^2)]^{1/2}k$ is made dimensionless with respect to the correlation length. $\tilde{T}$ is the dimensionless fluctuating stress contribution,

$$\tilde{T} = \mathbf{ll}:\frac{\partial}{\partial \hat{\phi}}\hat{\tau}'/(\eta_p^\circ\dot{\epsilon}) = 2(l_x^2 - l_y^2) + \mathrm{Wi}'(4 + 8R_\Psi') - 8\mathrm{Wi}^\circ(2 + 8R_\Psi^\circ)l_x^2 l_y^2 \tag{7}$$

The R_Ψ's are the ratios of the second to the first normal stress coefficients, and the Weissenberg numbers, Wi° and Wi', are given by $\mathrm{Wi}^\circ = \Psi_1^\circ\dot{\epsilon}/(2\eta_p^\circ)$ and $\mathrm{Wi}' = \Psi_1'\dot{\epsilon}/(2\eta_p^\circ)$, respectively. Approaching the coexistence curve, O_s increases and consequently the stress contribution to the structure factor increases as flow-enhanced concentration fluctuations are suppressed less effectively by the decreasing osmotic pressure. An example of the deviation of the structure factor from steady state $\Delta S(\tilde{\mathbf{k}};\mathrm{Wi}^\circ) = S(\tilde{\mathbf{k}};\mathrm{Wi}^\circ) - S(\tilde{\mathbf{k}};0)$, as predicted by eq 6, is depicted in Figure 1. Both enhanced scattering on the axis of extension and the fourfold symmetry are visible. Finally, concentration fluctuations are convected away from the stagnation point, thus reducing time during which concentration fluctuations are enhanced. A recent modification to the HF model[3] relaxes the assumption that the stress-relaxation time is much less than the relaxation time of concentration fluctuations $1/(Dk^2)$ and predicts a reduction in structure factor at large scattering vector values, k. Then the appearance of flow-induced peaks in the scattering pattern is predicted at $k \approx 1/(D\tau_r)^{1/2}$.

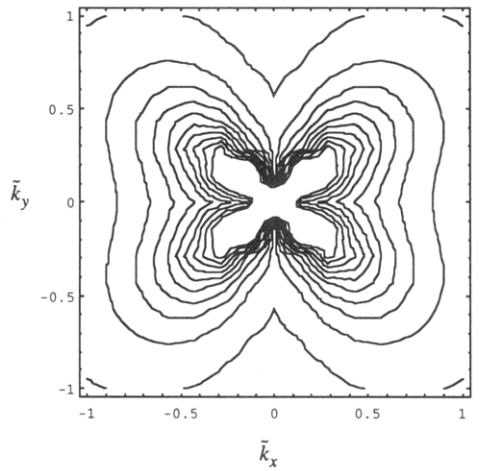

Figure 1. Steady-state structure factor $\Delta S(\tilde{\mathbf{k}},\mathrm{Wi})$ predicted from eq 6; $\mathrm{Wi}^\circ = \mathrm{Wi}' = 3$, $R_\Psi^\circ = R_\Psi' = -1/3$, $O_s = 0.1$.

Table I. Relaxation Times and Diffusion Coefficients

			D (μm^2 s^{-1})	
T (°C)	τ_s (s)	τ_r (s)	extension	shear[a]
20	0.3	0.4	0.05	0.04
16	1.3	1.0	0.04	0.02
14	2.2	3.2	0.03	0.015

[a] Reference 6.

3.0. Materials and Experimental Methods

Our sample consisted of a solution of PS/DOP with a volume fraction $\phi^\circ = 0.06$. The polystyrene had a molecular weight of $M_w = 1.86 \times 10^6$ and a polydispersity $M_w/M_n = 1.06$ and was obtained from Pressure Chemical Co. Since DOP is a poor solvent for PS at room temperature, the polymer was first dissolved in a small amount of chloroform. DOP was then added and the solution was made homogeneous by stirring for several days at a temperature of 50–60 °C. The chloroform was subsequently removed in a vacuum oven under a vacuum of 20 psi and a temperature of 60 °C. For this sample, the Θ temperature[32] is 22 °C while the cloud point lies between 10.0 and 10.5 °C.[1] All experiments were performed in a temperature range between 12 and 22 °C, between the cloud point and Θ temperature. Furthermore, the solution is semidilute, the overlap concentration being $\phi^* < 0.01$. The critical temperature for the PS/DOP system has been reported to be at $T_c = 11$ °C, with a critical concentration of $\phi_c = 0.02$.[1]

The characteristic rheological time scale τ_r was obtained from the relaxation of the first normal stress difference N_1 after cessation of simple shear flow. Then, by the stress-optical rule,[30] the relaxation time was determined from the exponential decay of intrinsic birefringence. Values for τ_r were accordingly determined from the zero shear limit in the linear regime of constant viscosity[9] and were found to be a function of temperature as detailed in Table I. This allowed for evaluation of the Weissenberg number $\mathrm{Wi} = \dot{\epsilon}\tau_r$ at various deformation rates.

Experiments were performed in a four-roll-mill flow cell (Figure 2) consisting of an arrangement of the four rotating cylinders, which were rotated by means of a Compumotor stepping motor with an angular precision of 25 000 steps/revolution. The relative motion of the four cylinders produces a plane extensional flow. Light propagates along the neutral axis parallel to the cylinders, thus allowing for light scattering by fluctuations in the plane of flow. The path length of the beam through the solution is $L =$ 2.8 cm. Temperature control to within 0.1 °C was achieved by pumping water through a heating/cooling coil surrounding the flow cell.

The SALS apparatus for measuring time-dependent SALS patterns has been extensively described in a previous paper.[6] Scattering dichroism and birefringence are measured simultaneously with SALS to complement observations of the structure of concentration fluctuations with the state of stress of the system.

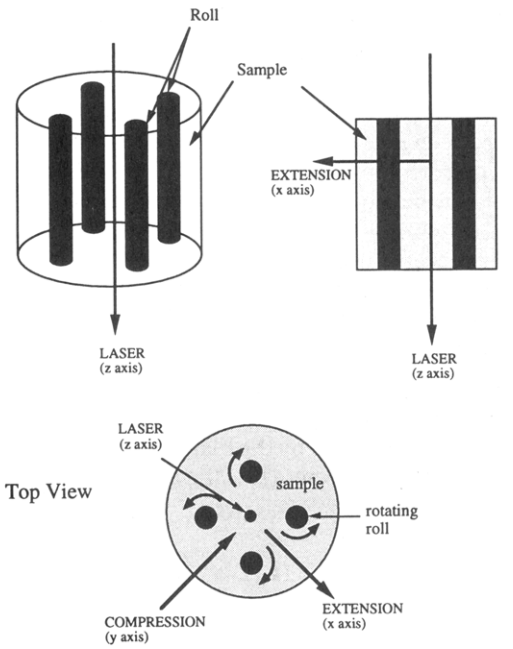

Figure 2. Four-roll-mill flow geometry.

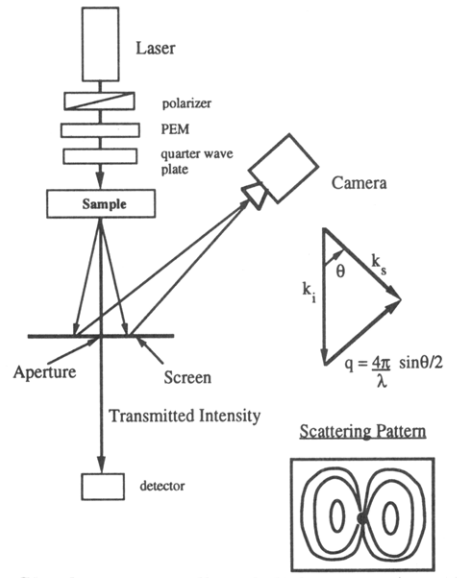

Figure 3. Simultaneous small-angle light scattering and dichroism apparatus.

The optical train (Figure 3) utilizes a polarization state modulation scheme to allow for time-dependent measurement of optical anisotropy.[33,34] Birefringence may be measured by installing a circular polarizer between the sample and the detector. For the determination of dichroism, the circular polarizer is removed.

Scattering is due to correlations in the fluctuation of the local dielectric tensor, and the scattering intensity is proportional to the structure factor. SALS may thus be used to probe the dynamics of concentration fluctuations. Intrinsic birefringence is due to anisotropy in the real part $n_{\alpha\beta}'$ of the refractive index tensor. Birefringence is related to the average polymeric stress through the stress-optical rule[30] $n_{\alpha\beta}' \sim \langle r_\alpha r_\beta \rangle \sim \tau_{\alpha\beta}$, where r_α is the polymer chain end-to-end vector. Although birefringence is the result of both intrinsic and form effects, the latter is dominated by intrinsic effects and can thus be neglected. On the other hand, dichroism is caused by anisotropy in the imaginary part of the refractive index tensor $n_{\alpha\beta}''$ and results in anisotropic attenuation of light. Dichroism in the present system arises only from form effects, which are due to scattering of light from anisotropic concentration fluctuations, and is related to the second moment of the structure factor $S(\mathbf{q})$ by the Onuki–Doi relation:[35]

$$n''_{\alpha\beta} = \frac{k^3}{32\pi^2\epsilon^{3/2}}\left(\frac{\partial\epsilon}{\partial c}\right)^2 \int d\Omega_{\hat{k}_s} (\delta_{\alpha\beta} - \hat{k}_{s_\alpha}\hat{k}_{s_\beta}) cS(\mathbf{q}) \quad (8)$$

where $\mathbf{q} = \mathbf{k}_s - \mathbf{k}_i$ is the scattering vector; $\mathbf{k}_i$ and $\mathbf{k}_s$ are the propagation vectors of incident and scattered light, respectively. $d\Omega_{\hat{k}_s}$ denotes solid angle integration over the unit vector $\hat{\mathbf{k}}_s$. In the limit of small ϵ, the anisotropic, flow-induced contribution to the structure factor of eq 3 results in a linear stress-optical relation between dichroism and fluctuating stress,

$$\eta''_{\alpha\beta} \sim \int d\Omega_{\hat{k}_s} (-\hat{k}_{s_\alpha}\hat{k}_{s_\beta}) l_\eta l_\vartheta \frac{\partial}{\partial\dot{\phi}}\dot{\gamma}_{\eta\vartheta}(\mathbf{q}) \quad (9)$$

For small-angle light scattering, the scattering vector $\mathbf{q}$ lies in the plane perpendicular to $\hat{\mathbf{k}}_i$. Hence $\mathbf{n}''$ has nonzero components only in the plane perpendicular to $\hat{\mathbf{k}}_i$. These components form a two-dimensional tensor, $\mathbf{n}''$. We introduce a Cartesian set of coordinates in q-space with q_z in the direction $-\hat{\mathbf{k}}_i$ and q_x in the direction of extension. The integration in eq 8 thus reduces to one over a square region of the q_x–q_y plane. The difference between the two principal values of $\mathbf{n}''$ finally gives the scattering dichroism $\Delta n''$,[34] while the angle of orientation of the dichroism χ'' is defined by the direction of the major axis of $\mathbf{n}''$. The detailed procedure for the evaluation of $\Delta n''$ and χ'' is described in our previous paper.[6] The angle of dichroism corresponds to the average orientation of the major axis of anistropic concentration fluctuations and by the Onuki–Doi relation is perpendicular to the orientation of the major axis of the anisotropic structure factor.[6] By eq 9, the orientation of concentration fluctuations is determined by the direction of long-wavelength fluctuating stresses. Alternatively, the direction of greatest concentration gradient is parallel to the direction of short-wavelength stresses. Along the axis of scattering dichroism χ'', scattering intensities are small. Hence we label this axis as the minor axis of the scattering pattern.

On application of the flow field, the scattering pattern deforms from its quiescent value. We define the deviation in the structure factor as $\Delta S(\mathbf{q},t;\dot{\gamma}) \equiv S(q,t;\dot{\gamma}) - S(\mathbf{q},0;0)$. In general, peaks appear near the major axis of $\Delta S(\mathbf{q},t;\dot{\gamma})$, their position depending on time, temperature, and rate of extension. These peaks correspond to the dominant q-mode of flow-enhanced concentration fluctuations, at a characteristic scattering magnitude q_c as defined in our previous paper.[6]

4.0. Results and Discussion

Time-dependent evolution of $S(\mathbf{q})$ and $\Delta n''$, including response to inception of steady extensional flow and relaxation on flow cessation, was measured using our simultaneous SALS and scattering apparatus. Experiments were conducted for extensional rates ranging from 0.2 to 20 s^{-1} and temperatures ranging from 12 to 22 °C. Under these conditions, PS/DOP is shear-thinning for Wi < 1 but becomes shear-thicknening for Wi ≫ 1. Viscosities are greater than 20 Pa·s,[10] thus ensuring Reynolds numbers of less than 0.1.

Evolution of the structure factor $S(\mathbf{q})$ in the flow field is visualized by a series of contour plots. As an example, Figure 4 presents the time evolution of $\Delta S(\mathbf{q})$ in plane extensional flow at a temperature of 12 °C and an extensional rate of 3 s^{-1}. Inception of flow is at t = 0 s, while cessation is at t = 20 s. The axis of extension is along the axis at 135° to the horizontal. The cross hairs on each contour plot indicate orientations of the major and minor axes given by the long and short lines and calculated respectively from eqs 27 and 21 of our previous paper.[6] The scattering pattern evolves anisotropically. At 1.0 s after inception of flow, two large lobes in $\Delta S(\mathbf{q})$ appear on the axis of extension (Figure 4a). Superimposed on the two-lobe pattern are four peaks arranged in a fourfold symmetric pattern, which is oriented at 45° to the direction of extension. Before steady state is reached, an intensity overshoot is observed (Figure 4b). Comparing scattering patterns just before (Figure 4d) and after flow cessation (Figure 4e), the scattered intensity suddenly increases after cessation before $\Delta S(\mathbf{q})$ relaxes to zero (Figure 4f). The steady-state structure factor (Figure 4d) is thus in agreement with the predictions of eq 6: a four-lobed pattern oriented at 45° to the principal axes of stress appears, and flow-enhanced scattering is parallel to the axis of extension, while perpendicular to this axis, scattering is suppressed.

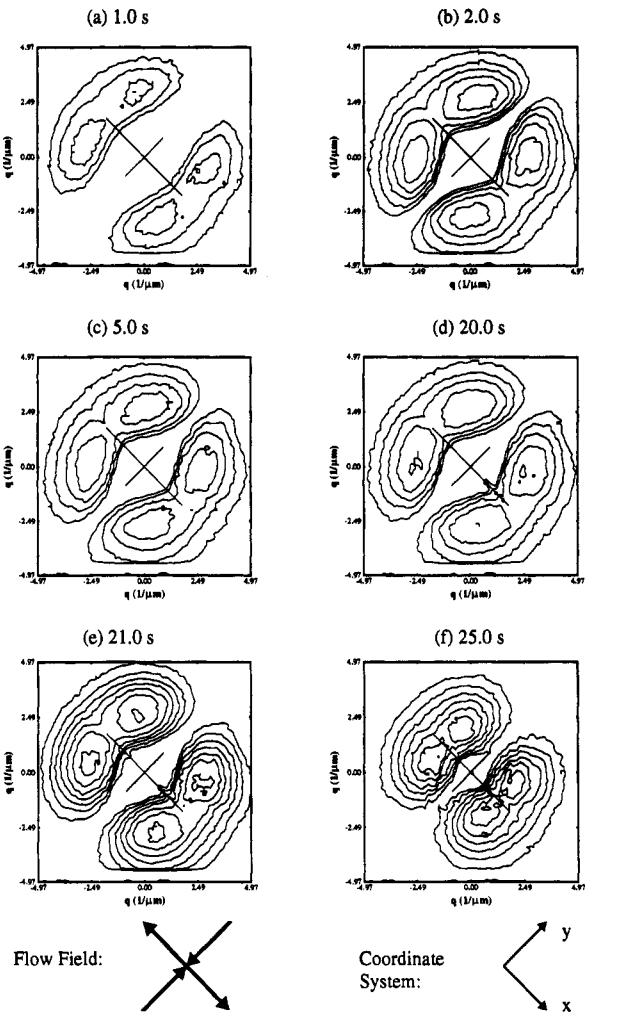

Figure 4. Time-dependent response of the structure factor $\Delta S(\mathbf{q})$ to steady extensional flow. Inception of flow corresponds to t = 0 s; cessation of flow is at t = 20 s; T = 14 °C, $\dot{\epsilon}$ = 3 s^{-1}. (a) t = 1.0 s; (b) t = 2.0 s; (c) t = 5.0 s (steady state); (d) t = 20.0 s; (e) t = 21.0 s; (f) t = 25.0 s.

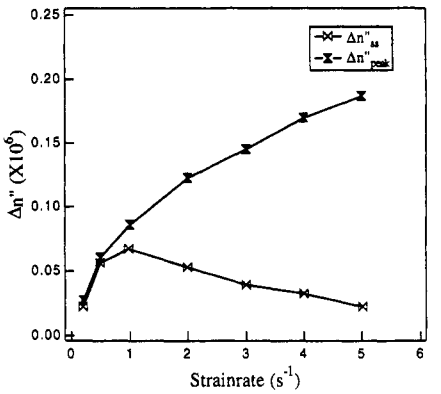

Figure 5. Steady-state dichroism $\Delta n''_{ss}$ and maximum overshoot $\Delta n''_{peak}$ vs $\dot{\epsilon}$; T = 14 °C.

Results for steady-state scattering dichroism $\Delta n_{ss}''$ are presented in Figure 5. As flow-induced fluctuations grow and align in the flow field with increasing extensional rate, dichroism increases. The angle of dichroism χ'' is fixed

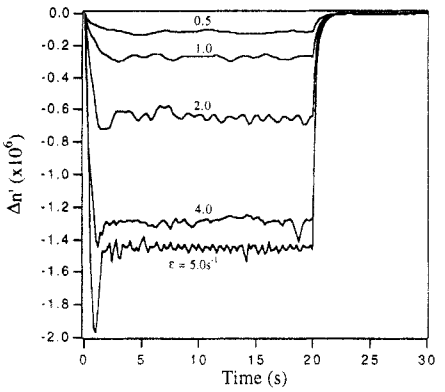

Figure 6. Birefringence $\Delta n'$ as a function of time; inception of flow corresponds to $t = 0$ s; cessation of flow is at $t = 20$ s; $T = 14$ °C.

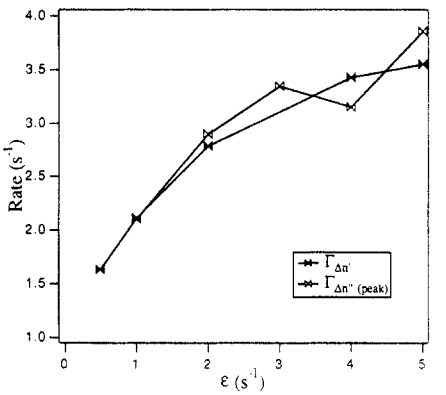

Figure 7. Characteristic rate for dichroism during overshoot at flow cessation $\Gamma_{\Delta n''}$ peak and characteristic rate for birefringence relaxation $\Gamma_{\Delta n'}$ vs $\dot{\epsilon}$; $T = 14$ °C.

perpendicular to the axis of extension (45°). At higher extensional rates, normal stresses dominate and eq 4 predicts an increase in scattering at all angles as well as an increase in the scattering in the four-lobed pattern. Dichroism relaxes on cessation of flow due to cooperative diffusion and a coupling of stress with flow-induced concentration fluctuations. Thus two time scales for relaxation are expected. $\Delta n''$ displays an overshoot peak shortly after flow cessation, believed to be due to concentration fluctuations coupling to a recoil in stress. This overshoot has been observed to occur over the same time scale τ_r as that of stress relaxation,[9] and similar overshoots have been observed on cessation of simple shear.[6] For Wi > 3, the steady-state dichroism decreases with increasing $\dot{\epsilon}$, but the peak value attained due to overshoot increases (Figure 5). Birefringence and hence polymeric stress increases with increasing $\dot{\epsilon}$, as shown in Figure 6. Moreover, as is evident from Figure 7, there is a correspondence between the fast time scale associated with the dichroism overshoot and the rate of birefringence relaxation $\Gamma_{\Delta n'}$. It appears then that stress recoil is probably responsible for the overshoot, especially since the fluctuating stress τ' lies at the root of flow-enhanced concentration fluctuations (eq 4). At low extensional rates the overshoot vanishes, presumably because of decoupling between stress and structure in the linear regime.

The Onuki–Doi theory[35] relating dichroism to the second moment of $S(\mathbf{q})$ (eq 8) has already been shown to be applicable for steady-state values of $\Delta n''$ in simple shear.[6] Dichroism $\Delta n''$ determined from the optical anisotropy of the transmitted beam and $\Delta n''_{SALS}$ as calcualted from scattering patterns by using eq 8 have been measured using the simultaneous SALS/dichroism apparatus. As shown in Figure 8, $\Delta n''_{SALS}$ and $\Delta n''$ correspond closely on flow

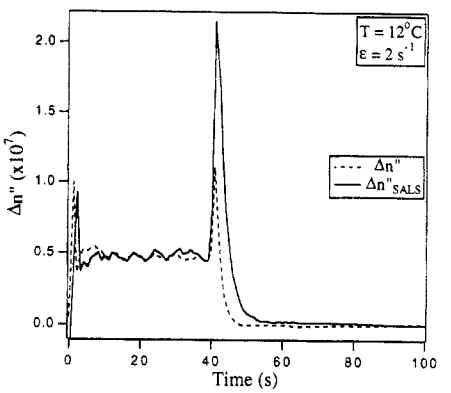

Figure 8. Dichroism $\Delta n''_{SALS}$ and $\Delta n''$ vs time; inception of flow corresponds to $t = 0$ s; cessation of flow is at $t = 20$ s; $T = 12$ °C, $\dot{\epsilon} = 2$ s^{-1}.

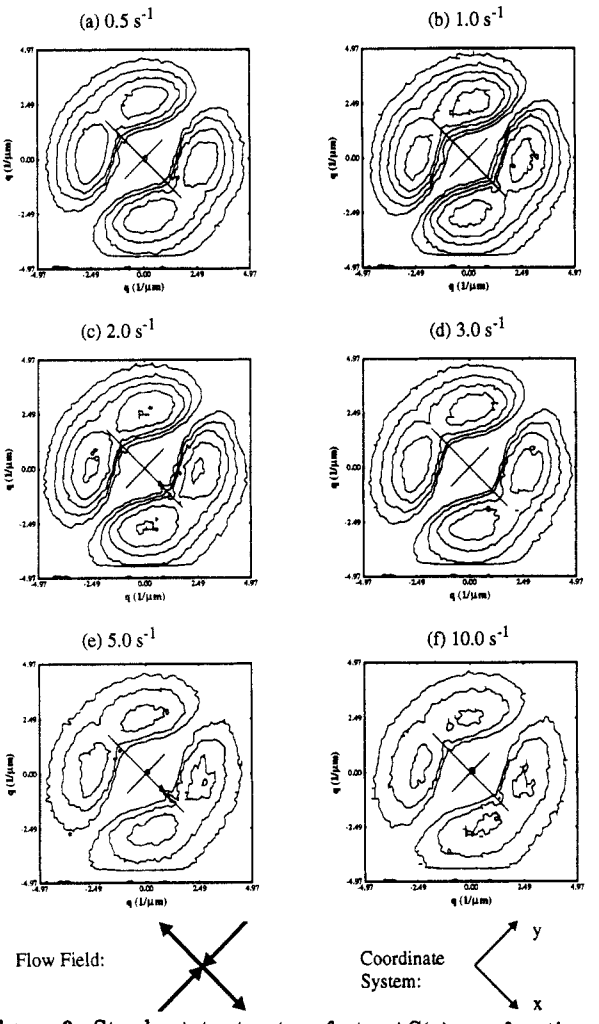

Figure 9. Steady-state structure factor $\Delta S(\mathbf{q})$ as a function of extensional rate $\dot{\epsilon}$; $T = 14$ °C. (a) $\dot{\epsilon} = 0.5$ s^{-1}; (b) $\dot{\epsilon} = 1.0$ s^{-1}; (c) $\dot{\epsilon} = 2.0$ s^{-1}; (d) $\dot{\epsilon} = 3.0$ s^{-1}; (e) $\dot{\epsilon} = 5.0$ s^{-1}; (f) $\dot{\epsilon} = 10.0$ s^{-1}.

inception at steady state, but less for the relaxation behavior on cessation of flow. The discrepancy in the overshoot peak may be a result of depolarization scattering contributions to $\Delta S(\mathbf{q})$ due to the formation of large associations such as gel-like particles, as discussed below. The dependence of steady-state $\Delta S(\mathbf{q})$, $\Delta n''_{SALS}$, and $\Delta n''$ on $\dot{\epsilon}$ is presented in Figures 9 and 10, where $\Delta n''_{SALS}$ has been multiplied by a single proportionality factor to obtain a best fit. At low $\dot{\epsilon}$, dichroism increases with $\dot{\epsilon}$, in agreement with eq 4. At high $\dot{\epsilon}$, dichroism decreases linearly with increasing extensional rate. This may be due to a decreased time available for coupling between flow field and concentration fluctuations. However, if this were the case,

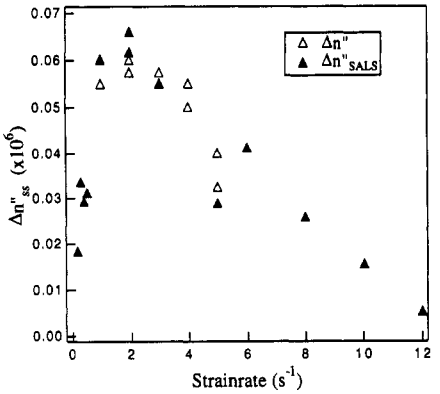

Figure 10. Steady-state $\Delta n''_{SALS}$ and $\Delta n''$ vs $\dot{\epsilon}$; T = 14 °C.

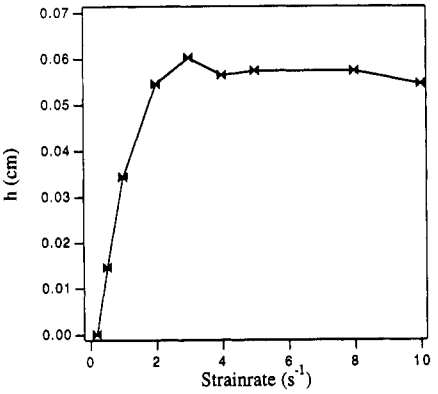

Figure 11. Steady-state turbidity h vs $\dot{\epsilon}$; T = 14 °C.

the overshoot peak should also decrease. Despite this decrease in steady-state anisotropy, the maximum of the overshoot in dichroism increases with $\dot{\epsilon}$ (Figure 5). This agrees with the assumption that the overshoot is related to a recoil of the stored elastic stresses. Steady-state flow-induced turbidity characterized by the extinction coefficient h, defined in our previous paper,[6] is presented in Figure 11.

Since flow enhancement of concentration fluctuations depends on the osmotic pressure, structure factors are temperature dependent. At temperatures near the coexistence curve, fluctuations are more readily enhanced, while at high temperatures greater extensional rates are required to achieve flow-enhanced scattering (Figure 12).

The q-dependent behavior of $\Delta S(\mathbf{q})$ is similar to that for steady shear as shown by Figures 10 and 12 of our previous paper.[6] On inception of flow, a peak appears in $\Delta S(\mathbf{q})$ along the major axis at large q. The q value for this peak is denoted by q_{max}. As steady state is reached, the peak grows in intensity and q_{max} decreases to a value of approximately 3.5 μm^{-1}. On cessation of shear, $\Delta S(\mathbf{q})$ rapidly increases for all values of q due to the stress recoil and then relaxes to zero due to diffusion. The time-dependent behavior of q_{max} and q_c is plotted in Figure 13. After the flow-cessation overshoot of $\Delta S(\mathbf{q})$, each mode relaxes exponentially with a relaxation time $\tau(q)$:

$$\tau(q) = \tau_s + \frac{1}{Dq^2} \tag{10}$$

where D is the cooperative diffusion coefficient and τ_s is a stress relaxation time. Relaxation is then due to a coupling between stress relaxation and cooperative diffusion. Equation 10 corresponds to the slow relaxation mode for concentration fluctuations as predicted by Brochard and de Gennes (BG).[36,37] The relative intensity of the fast mode of BG would be too small to be detected.[37,38] For shear experiments, eq 10 has also been

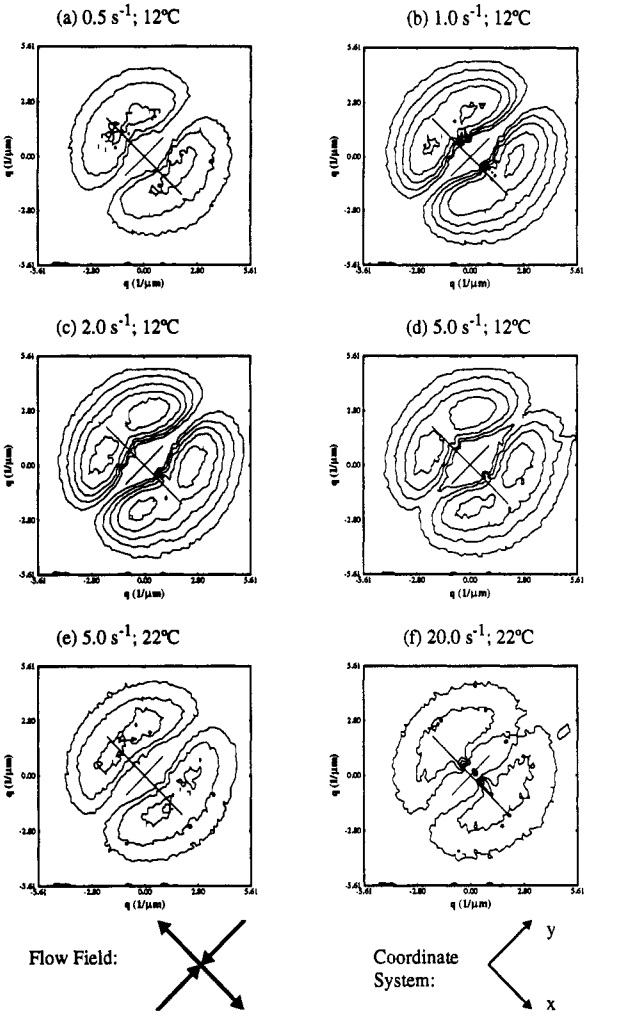

Figure 12. Steady-state structure factor $\Delta S(\mathbf{q})$ as a function of extensional rate $\dot{\epsilon}$ and temperature. (a) $\dot{\epsilon}$ = 0.5 s^{-1}, T = 12 °C; (b) $\dot{\epsilon}$ = 1.0 s^{-1}, T = 12 °C; (c) $\dot{\epsilon}$ = 2.0 s^{-1}, T = 12 °C; (d) $\dot{\epsilon}$ = 5.0 s^{-1}, T = 12 °C; (e) $\dot{\epsilon}$ = 5.0 s^{-1}, T = 22 °C; (f) $\dot{\epsilon}$ = 20.0 s^{-1}, T = 22 °C.

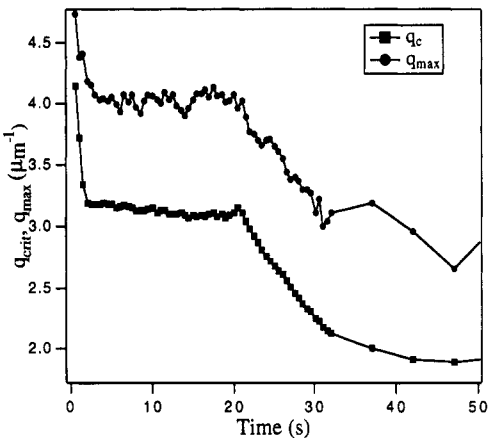

Figure 13. q_{max} and q_c vs time for the Couette geometry; T = 14 °C, $\dot{\epsilon}$ = 2 s^{-1}.

shown to be a good predictor of relaxation time.[6,38] For T = 14 °C and $\dot{\epsilon}$ = 2 s^{-1} we determine τ_s = 2.2 s, which is similar to the characteristic relaxation time at this temperature; τ_r = 3.2 s (see Table I). The cooperative diffusion coefficient was found to be approximately 0.03 μm^2 s^{-1}.

A new development is the discovery of significant depolarization scattering as observed by placing the flowing system between crossed polarizers. Structures responsible for this scattering are large and correspond to scattering

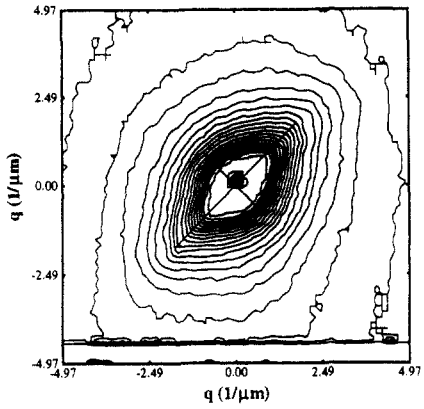

Figure 14. Steady-state lozenge scattering pattern; $T = 14$ °C.

angles smaller than q_{max}. Depolarization scattering is the result of large correlations between the local anisotropic contribution to the refractive index tensor and are usually observed in dense systems such as polymeric solids.[31] Moreover, we observed depolarization scattering patterns are in the form of "lozenges" (Figure 14), similar in shape to those observed by Boue and co-workers[39] for deformed gels. We speculate that concentration fluctuation enhancement may be a precursor to polymeric associations such as gel-like particles.

Acknowledgment. This research has been funded by a grant from the NSF (Grant DMR 9120360). The authors thank R. G. Larson for rewarding discussions on the topics presented in this paper.

References and Notes

(1) Rangel-Nafaile, C.; Metzner, A. B.; Wissbrun, K. F. *Macromolecules* **1984**, *17*, 1187.
(2) Tirrell, M. *Fluid Phase Equilib.* **1986**, *30*, 367.
(3) Larson, R. G. *Rheol. Acta* **1992**, *31*, 497.
(4) Ver Strate, G.; Philippoff, W. *J. Polym. Sci., Polym. Lett. Ed.* **1974**, *12*, 267.
(5) Wu, X.-L.; Pine, D. J.; Dixon, P. K. *Phys. Rev. Lett.* **1991**, *66*, 2408.
(6) van Egmond, J. W.; Werner, D. E.; Fuller, G. G. *J. Chem. Phys.* **1992**, *96*, 7742.
(7) Hashimoto, T.; Fujioka, K. *J. Phys. Soc. Jpn.* **1991**, *60*, 356.
(8) Nakatani, A. L.; Waldow, D. A.; Han, C. C. *Proc. ACS/PSME* **1991**, *65*, 216.
(9) van Egmond, J. W.; Fuller, G. G. *Rheol. Acta*, submitted.
(10) Yanase, H.; Moldenaers, P.; Mewis, J.; Abetz, V.; van Egmond, J. W.; Fuller, G. G. *Rheol. Acta* **1991**, *30*, 89.
(11) Frank, F. C.; Keller, A.; Mackley, M. R. *Polymer* **1971**, *12*, 467.
(12) McHugh, A. J.; Forrest, E. H. *J. Macromol. Sci., Phys.* **1975**, *B11*, 219.
(13) Peterlin, A. *Polym. Eng. Sci.* **1976**, *16*, 126.
(14) Stein, R. *Polym. Eng. Sci.* **1976**, *16*, 152.
(15) Katsaros, J. D.; Malone, M. F.; Winter, H. H. *Polym. Bull.* **1986**, *16*, 83.
(16) Keller, A.; Odell, J. A. *Colloid Polym. Sci.* **1985**, *263*, 181.
(17) Fuller, G. G.; Leal, L. G. *J. Polym. Sci., Polym. Phys. Ed.* **1981**, *19*, 557.
(18) Geffroy, E.; Leal, L. G. *J. Polym. Sci., Polym. Phys. Ed.* **1992**, *30*, 1329.
(19) Helfand, E.; Fredrickson, G. H. *Phys. Rev. Lett.* **1989**, *62*, 2468.
(20) Onuki, A. *Phys. Rev. Lett.* **1989**, *62*, 2472.
(21) Onuki, A. *J. Phys. Soc. Jpn.* **1990**, *59*, 3423.
(22) Onuki, A. *J. Phys. Soc. Jpn.* **1990**, *59*, 3427.
(23) Doi, M. In *Dynamics and Patterns in Complex Fluids*; Onuki, A., Kawasaki, K., Eds.; Springer-Verlag: Berlin, 1990.
(24) Doi, M.; Onuki, A. *J. Phys. II* **1992**, *2*, 1631.
(25) Milner, S. T. *Phys. Rev. Lett.* **1991**, *66*, 1477.
(26) de Gennes, P.-G. *Macromolecules* **1974**, *9*, 587.
(27) Hohenberg, P. C.; Halperin, B. I. *Rev. Mod. Phys.* **1977**, *49*, 435.
(28) de Gennes, P.-G. *Scaling Concepts in Polymer Physics*; Cornell University Press: Ithaca, NY, 1979.
(29) Larson, R. G. *Constitutive Equations for Polymer Melts and Solutions*; Butterworths: Boston, 1988.
(30) Doi, M.; Edwards, S. F. *The Theory of Polymer Dynamics*; Oxford University Press: Oxford, 1986.
(31) Berne, B. J.; Pecora, R. *Dynamic Light Scattering*; Wiley: New York, 1976.
(32) Park, J. O.; Berry, G. C. *Macromolecules* **1989**, *22*, 3022.
(33) Fuller, G. G.; Mikkelsen, K. J. *J. Rheol.* **1989**, *33*, 761.
(34) Fuller, G. G. *Annu. Rev. Fluid Mech.* **1990**, *22*, 384.
(35) Onuki, A.; Doi, M. *J. Chem. Phys.* **1986**, *85*, 1190.
(36) Brochard, F.; de Gennes, P.-G. *Macromolecules* **1977**, *10*, 1157.
(37) Brochard, F. *J. Phys.* **1983**, *44*, 39.
(38) Dixon, P. K.; Pine, D. J.; Wu, X.-L. *Phys. Rev. Lett.* **1992**, *68*, 2239.
(39) Boue, F.; Bastide, J.; Buzier, M.; Lapp, A.; Herz, J.; Vilgis, T. A. *J. Polym. Colloid Sci.* **1991**, *269*, 195.